

# Extended hydrodynamic description for nonequilibrium atom-surface interactions

D. Reiche,<sup>1,2</sup> M. Oelschläger,<sup>1,2</sup> K. Busch,<sup>1,2</sup> and F. Intravaia<sup>1</sup>

<sup>1</sup>*Humboldt-Universität zu Berlin, Institut für Physik,  
AG Theoretische Optik & Photonik, 12489 Berlin, Germany*  
<sup>2</sup>*Max-Born-Institut, 12489 Berlin, Germany*

The dissipative properties of spatially nonlocal conductors are investigated in the context of quantum friction acting on an atom moving above a macroscopic body. The focus is on an extended version of the hydrodynamic model for the bulk material's electromagnetic response. It is shown that the standard hydrodynamic description is inadequate for evaluating the frictional force since it completely neglects Landau damping. The extended version of the model contains a frequency-dependent compressibility factor for the Fermi liquid and qualitatively resolves this issue. For a quantitative assessment, these results are contrasted with those obtained for the more fundamental Boltzmann-Mermin model. Since the latter is technically involved, the simplicity of the extended hydrodynamic model allows for an easier analysis of the impact of nonlocality on quantum friction for other (planar) geometries. This is illustrated with an example involving a thin slab.

## I. INTRODUCTION

One remarkable feature of quantum theory is the existence of zero-point fluctuations: Even in its state of minimal energy each quantum system is restless. These quantum fluctuations induce macroscopic consequences in the form of experimentally accessible dispersion forces. One prominent representative of such forces is the Casimir effect [1] which, in its original form, is characterized by an attraction between two electrically neutral, non-magnetic bodies placed in vacuum. Over the past decade, another class of quantum-fluctuation-induced phenomena has been intensively investigated. The accent is placed on the non-conservative aspect of the interaction. For instance, when spatially separated objects are set in motion relative to each other, a fluctuation-induced drag force appears and counteracts the dynamics. This nonequilibrium scenario is usually referred to as quantum or Casimir friction [2–8]. The frictional interaction strongly depends on the optical response of the materials composing the objects in the system. Specifically, in dynamical nonequilibrium, dispersion forces have shown to be very sensitive to the materials' dissipative characteristics [9, 10]. On the one hand, this means that precise predictions for experimental studies of nonequilibrium dispersion forces inevitably call for the use of reliable and well-understood models of the material's optical response. On the other hand, this discloses the potential of these interactions for usage in (quantum) sensing and other technological applications.

Quantum friction between an atom and a planar surface was investigated in the case of spatially dispersive conductors in Refs. [11, 12]. It was pointed out that, when the atom-surface separation  $z_a$  becomes comparable to the bulk electron's mean free path  $\ell$ , Landau damping [13] plays an important role in determining the strength of the interaction. In addition to modifying the functional dependence of the force on  $z_a$ , Landau damping is responsible for a considerable enhancement of the interaction strength as compared to a local description

that would only feature collision-induced damping (i.e., the Drude model [14]). These results have been obtained by describing the reflection coefficients of the metal in the framework provided by the semi-classical infinite barrier (SCIB) approximation [15]. The dielectric functions were modeled using the Lindhard approach [16] including Mermin correction [17] in the limit of wave vectors smaller than the Fermi wave vector. Equivalently, one could have used a semi-classical approach relying on the Boltzmann equation and involving the zero-temperature Fermi-Dirac distribution for describing the properties of the electrons in the material. This is why the reported enhancement of the frictional force is sometimes referred to as originating from the *Boltzmann-Mermin model* [18]. Due to its complexity, however, the Boltzmann-Mermin description is not the most practical approach for describing nonlocal electromagnetic interactions. Numerous studies analyzing spatial dispersion in nanophotonic systems use the less complex *hydrodynamic model*, which describes the electrons in the medium in terms of a charged and compressible fluid. Although it might be sufficient for some calculations involving nanostructured objects, the hydrodynamic model provides a rather rough description of the actual physics of the system. For example, in its simplest but commonly adopted variant, it does not include Landau damping. In order to preserve its appealing simplicity without neglecting important physical characteristics, the hydrodynamic model has been extended in many ways ( see Refs. [19–22]).

In this manuscript, we consider a specific modification of the hydrodynamic equations which focuses on the compressibility factor  $\beta$  of the electronic fluid [19] (see Sec. II). Instead of being a real constant as in the standard treatment, the compressibility becomes a complex function of the frequency of the electromagnetic radiation. In the context of atom-surface quantum friction (Sec. III), we compare this extended hydrodynamic model to the Boltzmann-Mermin model on the level of the reflection coefficients for both, a planar interface to an infinitely extended body (Sec. III A) and a finite-sized planar slab (Sec. III B). Specifically, we provide a detailed under-

standing in terms of physical processes and connect our findings to the material's dissipative processes which for metals coincide with their *resistivity*. Based on this, we study the impact of the two models on quantum frictional forces and assess their range of validity. We close our discussion with a summary and further remarks (Sec. IV).

## II. MODELS FOR SPATIAL DISPERSION

The description of a spatially nonlocal material and its optical response at the interface with vacuum or another dielectric has been investigated in various contexts by many authors (see for example Refs. [16, 20, 23–33]). While in the abstract configuration of an infinite bulk material the symmetry of the system allows for a self-consistent description of the dynamics, this turns out to be considerably more difficult as soon as an interface occurs. With a nonlocal description of the material, additional boundary conditions (ABCs) of non-electromagnetic origin are often required for a complete characterization of the system's optical response. The two models considered in our work are no exception. In order to obtain the reflection coefficients for a planar medium, we follow the SCIB approach which induces an ABC that is equivalent to the specular reflection of electrons at the interface. The bulk optical response is connected to the interface impedance by the relations [15]

$$Z^{\text{TM}}(\omega, p) = \frac{2ic}{\pi\omega} \int_0^\infty \frac{dq}{k^2} \left[ \frac{q^2}{\epsilon_l(\omega, k) - \frac{c^2 k^2}{\omega^2}} + \frac{p^2}{\epsilon_l(\omega, k)} \right], \quad (1a)$$

$$Z^{\text{TE}}(\omega, p) = \frac{2ic}{\pi\omega} \int_0^\infty dq \frac{1}{\epsilon_t(\omega, k) - \frac{c^2 k^2}{\omega^2}}, \quad (1b)$$

where  $c$  is the vacuum speed of light and TE and TM describe the two polarizations of the electromagnetic radiation.  $\epsilon_l(\omega, k)$  and  $\epsilon_t(\omega, k)$  denote the nonlocal longitudinal and transverse (bulk) permittivities. They are functions of frequency  $\omega$  and, due to symmetry reasons, of the modulus of three-dimensional wave vector  $k^2 = p^2 + q^2$ , where  $p = \sqrt{p_x^2 + p_y^2}$  is the component parallel to the surface and  $q$  is the component orthogonal to it.

In previous work [12], we have used these expressions in conjunction with the permittivity functions given by the Boltzmann-Mermin model for a metal [15–17], which we report here for completeness:

$$\epsilon_l(\omega, k) = 1 + \frac{\omega_p^2}{\omega + i\Gamma} \frac{3u^2 g_l(u)}{\omega + i\Gamma g_l(u)}, \quad (2a)$$

$$\epsilon_t(\omega, k) = 1 - \frac{\omega_p^2}{\omega(\omega + i\Gamma)} g_t(u), \quad (2b)$$

where  $\omega_p$  is the plasma frequency of the metal and

$$g_l(u) = 1 - u \operatorname{arccoth}(u) \quad (3a)$$

$$g_t(u) = \frac{3}{2} [u^2 - (u^2 - 1)u \operatorname{arccoth}(u)] \quad (3b)$$

are dimensionless functions of the variable  $u = (\omega + i\Gamma)/(v_F k)$  defined in terms of the Fermi velocity  $v_F$  and the collision (dissipation) rate  $\Gamma$ . For simplicity, we are going to consider a constant value of  $\Gamma$  in the following. In general, however,  $\Gamma$  contains a temperature-dependent part connected with the type of collision (e.g. electron-electron, electron-phonon) [34, 35], as well as a temperature-independent part depending on the amount of defects or impurities present in the material [36, 37]. Eqs. (2) and (3) are also consistent with the assumption of a fully degenerated electron gas, valid for  $T \ll T_F$  ( $T_F \sim 10^5$  K). Based on the Lindhard framework [16], Eq. (2) includes the so-called Mermin correction [15, 17], but neglects effects occurring at scales below the electron's de Broglie wavelength,  $\lambda_B = 2\pi\hbar/(mv_F)$  (essentially the inverse of the Fermi wave vector and usually of the order of a few tenths of an angstrom), which are outside the range of validity of the theory. The local limit is obtained for  $|u| \rightarrow \infty$ , where both longitudinal and transverse permittivity coincide with the well-known spatially local Drude permittivity

$$\epsilon_{\text{Dr}} = 1 - \frac{\omega_p^2}{\omega(\omega + i\Gamma)}. \quad (4)$$

The strongest nonlocal corrections, however, occur for  $|u| \rightarrow 0$ : The dielectric functions show a nonzero complex part connected with the (mathematical) behavior of  $\operatorname{arccoth}[u]$  for  $u < 1$  even if no collision-induced damping is present ( $\Gamma \rightarrow 0$ ). Physically, the complex part corresponds to Landau damping. This phenomenon describes a situation where the phase velocity of the electromagnetic wave in the electron gas matches or is less than the electrons' speed, i.e.  $\omega/k \leq v_F$  allowing for the transfer of the electromagnetic fields energy to the electrons.

As explained above, the focus of our work lies on the so-called hydrodynamic model. It derives from a description of the electrons in the bulk as quasi-particle excitations of a charged and compressible fluid. The quasi-particle excitations are supposed to obey both, charge conservation (continuity equation) and momentum conservation. The latter is described by means of the Euler equation including collision-induced damping and the Fermi pressure (originating from the Pauli exclusion principle) under the influence of the external Lorentz force [38]. In its linearized version, the permittivity functions for the hydrodynamic model are given by the rather simple expressions

$$\epsilon_l(\omega, k) = 1 - \frac{\omega_p^2}{\omega(\omega + i\Gamma) - \beta^2 k^2}, \quad (5a)$$

$$\epsilon_t(\omega, k) = 1 - \frac{\omega_p^2}{\omega(\omega + i\Gamma)}. \quad (5b)$$

Notice that in this description only the longitudinal permittivity is affected by nonlocality, while the transverse one is identical to the common local expression given by the Drude model, i.e.  $\epsilon_t(\omega, k) \equiv \epsilon_{\text{Dr}}(\omega)$  [14]. In contrast to the Boltzmann-Mermin model, only the TM polarized reflection coefficient is modified relative to its local counterpart [see Eq. (1)]. The most important parameter of the hydrodynamic description is the compressibility of the electron fluid, described by  $\beta$ , which in our case is connected to the Fermi pressure [19]. In the literature, authors have chosen different values for this parameter, the most popular being  $\beta^2 = v_F^2/3$  and  $\beta^2 = 3v_F^2/5$ . They correspond to different frequency limits (low frequency – Thomas-Fermi description [39] and high frequency, respectively) in the implicit assumptions which lead to the hydrodynamic equations of motion of a degenerate electron gas (for instance, see Refs. [19, 40, 41]). Independent of its precise value, however, as long as  $\beta$  stays real, the imaginary part of the permittivity is intrinsically connected with the collision-induced damping  $\Gamma$  only. For  $\Gamma = 0$ , apart from a resonant exchange of energy occurring at  $\omega/k = \beta$ , the dielectric function describes a system lacking dissipation.

With the aim of providing a more fundamental background for the hydrodynamic description, P. Halevi suggested to compare the two models, i.e. the Boltzmann-Mermin and hydrodynamic model [19]. In particular, by equating the two longitudinal permittivities in Eq. (2) and Eq. (5), we obtain

$$\frac{\beta^2}{v_F^2} = \frac{\omega \left[ u^2 + \frac{1}{3g_l(u)} \right] + i\frac{\Gamma}{3}}{\omega + i\Gamma}. \quad (6)$$

An expansion in  $1/|u|$  gives at the leading order the complex and frequency-dependent compressibility factor,

$$\beta^2(\omega) \approx \frac{\frac{3}{5}\omega + \frac{1}{3}\Gamma}{\omega + i\Gamma} v_F^2. \quad (7)$$

This function introduces an additional phase between the plasma oscillations and the electromagnetic radiation. It also adequately reproduces the limiting values of  $\beta$  for the low and high frequency limit, respectively. Interestingly enough, despite the fact that the expansion in  $1/|u|$  is consistent with a limit of weak spatial dispersion, some features of the Landau damping are preserved as long as the collisional damping is large enough. Indeed from  $1/|u| \ll 1$ , we obtain

$$\sqrt{v_F^2 - \frac{\Gamma^2}{k^2}} \ll \frac{\omega}{k} \leq v_F, \quad (8)$$

which sets a lower bound to the validity of the approximation in terms of the phase velocity of the electromagnetic field. More importantly, it shows that the approximation (7) still allows for waves with a phase velocity smaller than the electrons' speed, hence allowing for Landau damping. Since Landau damping plays a significant

role in quantum friction at small atom-surface separations, it is interesting to analyze the impact of Eq. (7) on the drag force. We study whether the extension to the usual hydrodynamic model proposed by Halevi can reproduce the features of the more fundamental Boltzmann-Mermin model. Finally, we like to note that recently Mortensen et al. [20] have suggested a similar extension of the standard hydrodynamic model via a complex compressibility coefficient in order to capture the physics of nano-gap structures in numerical evaluations.

### III. ATOM-SURFACE QUANTUM FRICTION

For our purpose, it is convenient to briefly review the theory of quantum friction. We refer to the literature for more details (for instance, see Refs. [10, 42, 43]). Throughout the manuscript we assume for simplicity that system is at zero temperature. For an atom or another microscopic object (nano-particle) moving in vacuum at constant velocity  $\mathbf{v}$  and constant height  $z_a$  above a flat surface, the quantum frictional force  $\mathbf{F}$  is given by [43, 44]

$$\mathbf{F} = -2 \int_0^\infty d\omega \int \frac{d^2\mathbf{p}}{(2\pi)^2} \times \mathbf{p} \text{Tr} [\underline{S}(\mathbf{p} \cdot \mathbf{v} - \omega, \mathbf{v}) \cdot \underline{G}_I(\mathbf{p}, z_a, \omega)]. \quad (9)$$

The subscript  $I$  indicates the imaginary part of the corresponding quantity.  $\underline{S}(\omega, \mathbf{v})$  is the velocity-dependent atomic power spectrum and  $\underline{G}$  is the Fourier transform with respect to the planar coordinates of the electromagnetic Green tensor. For a flat surface, the expression of the latter can be given in terms of a linear combination of the transverse electric and magnetic reflection coefficients [45] [see Eqs. (14) and (22)]. For simplicity, in Eq. (9) we model the moving particle as a rigid dipole  $\hat{\mathbf{d}}(t) = \mathbf{d}\hat{q}(t)$ , where  $\mathbf{d}$  is the static dipole vector and  $\hat{q}(t)$  describes the dipole's internal dynamics. Although quantum friction shares many aspects with the equilibrium Casimir-Polder interaction, it clearly displays features which are specific of a non-conservative interaction. Specifically, the drag force is strongly connected with the system's dissipative behavior. In our setup, dissipation can arise in (i) the macroscopic material of the surface and (ii) the particle's internal degrees of freedom. For the metallic surface (i), this points to the collision-induced damping and, if present, to Landau damping of the electron fluid. In the case of the moving microscopic object (ii), the origin of dissipation is different depending on whether the particle features some form of internal dissipation (as it is the case, e.g., for a metallic nanoparticle) or whether the damping is induced by the interaction with the electromagnetic field only, as it is the case in an atomic system. In this work, we only consider the latter case, where the radiation dressing, backaction and their interplay with the surface characterize the interaction between atom and surface [46]. If the internal dynamics is

described in terms of a harmonic oscillator, the atomic power spectrum reads as

$$\underline{S}(\omega, \mathbf{v}) = \frac{\hbar}{\pi} \int \frac{d^2 \tilde{\mathbf{p}}}{(2\pi)^2} \theta(\omega + \tilde{\mathbf{p}} \cdot \mathbf{v}) \times \underline{\alpha}(\omega, \mathbf{v}) \cdot \underline{G}_I(\tilde{\mathbf{p}}, z_a, \omega + \tilde{\mathbf{p}} \cdot \mathbf{v}) \cdot \underline{\alpha}^*(\omega, \mathbf{v}), \quad (10)$$

where  $\underline{\alpha}(\omega, \mathbf{v})$  is the velocity-dependent atomic polarizability and  $\theta(\omega)$  is the Heaviside step function [46].

In our non-relativistic description, quantum friction on atoms originates from the interaction at frequencies  $0 \leq \omega \lesssim v/z_a$  ( $v = |\mathbf{v}|$ ). Hence, for sufficiently low velocities, only the low-frequency features of the atomic power spectrum and the bulk material's optical response are of interest. For many practical cases, it is therefore sufficient to restrict the description of materials to their conducting properties. For typical velocities (speed of sound and slower), this corresponds to a frequency region where common materials (including those considered in our work) are Ohmic, i.e.  $r_I(\omega, k) \propto \omega$ . Under these circumstances and for a motion within the near field of the surface (strongest interaction), the force is well approximated by [12]

$$F \approx -2\hbar \frac{v^3}{\pi} \left( \frac{\Phi_0 \Phi_2}{3} \mathcal{D}_0(z_a) \mathcal{D}_2(z_a) + \Phi_1^2 \mathcal{D}_1^2(z_a) \right). \quad (11)$$

Here,  $\mathbf{F} = F\mathbf{v}/v$  and we have defined

$$\Phi_n = \binom{2n}{n} \frac{\frac{2n+1}{2(n+1)} \alpha_{xx} + \frac{1}{2(n+1)} \alpha_{yy} + \alpha_{zz}}{2^{2n+3} \pi \epsilon_0}, \quad (12a)$$

$$\mathcal{D}_n(z_a) = \int_0^\infty dp p^{2(n+1)} e^{-2z_a p} [\partial_\omega r_I^{\text{TM}}(\omega, p)|_{\omega=0}], \quad (12b)$$

where  $\epsilon_0$  denotes the vacuum permittivity. The constants  $\alpha_{ii}$  are the diagonal components of the static atomic polarizability tensor, which for our model is given by the dyadic  $\underline{\alpha}_0 = 2\mathbf{d}\mathbf{d}/\hbar\omega_a$  with  $\omega_a$  being the characteristic atomic transition frequency. The sign in Eq. (11) highlights that the force is oriented opposite to the direction of motion and, as expected, the definition of  $\mathcal{D}_n(z_a)$  shows that it is connected to the dissipative properties of the surface (imaginary part of the reflection coefficient). Notice that in the near-field limit, as long as the atom is described in terms of an electric dipole, the dominant contribution to the interaction is provided solely by the TM-polarized field. Further,  $\mathcal{D}_n(z_a)$  also defines the functional dependence of the frictional force on the atom-surface separation  $z_a$ . For a spatially local material, the reflection coefficients are independent of the wave vector and we find in the Ohmic regime  $[\partial_\omega r_I^{\text{TM}}(\omega)|_{\omega=0}] = 2\epsilon_0 \rho_{\text{lc}}$ , where  $\rho_{\text{lc}}$  is a constant related to dissipation in the material. For the local Drude conductor, the permittivity at low frequencies is asymptotic to  $\epsilon \sim i[\epsilon_0 \rho_{\text{lc}} \omega]^{-1}$ , where  $\rho_{\text{lc}} = \Gamma/(\epsilon_0 \omega_p^2)$  is the metal's resistivity. The integral in Eq. (12b) can be readily evaluated to

$$\mathcal{D}_n(z_a) = 2\epsilon_0 \rho_{\text{lc}} \frac{[2(n+1)]!}{(2z_a)^{2n+3}} \quad (13)$$

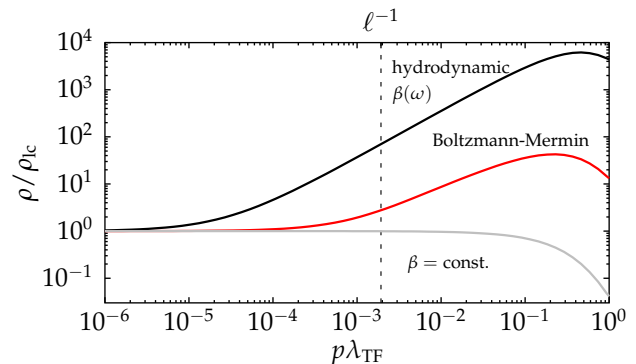


FIG. 1. The nonlocal resistivity  $\rho(p)$  as a function of the wave vector  $p$  and normalized to its local counterpart,  $\rho_{\text{lc}}$ , for the different models analyzed in the main text. Both, the Boltzmann-Mermin (red) and the extended hydrodynamic model with a frequency-dependent compressibility factor (black) feature a maximum in  $\rho(p)$  for  $p\lambda_{\text{TF}} \sim 1/5$  and  $p\lambda_{\text{TF}} \sim 1/2$ , respectively. The standard hydrodynamic description (gray) with constant and real  $\beta$  (here equal to  $v_F/\sqrt{3}$ ) corresponds to a  $\rho(p)/\rho_{\text{lc}}$  which tends to one for  $p\lambda_{\text{TF}} \ll 1$  and monotonically decreases to zero for  $p\lambda_{\text{TF}} \gg 1$ . Typical parameters for gold have been chosen, namely  $\Gamma = 30$  meV,  $\omega_p = 9$  eV [47] and  $v_F = \alpha_{\text{fs}} c$  with  $\alpha_{\text{fs}}$  the fine-structure constant.

demonstrating that  $F_{\text{lc}} \propto \rho_{\text{lc}}^2 v^3 / z_a^{10}$  [12].

### A. A nonlocal infinite half space

The above expressions also indicate how spatial dispersion can modify the frictional interaction. While the dependence on the velocity is essentially not affected by nonlocality, the force can be modified both, in its strength and in its functional dependence on the atom-surface separation through the expression for  $\mathcal{D}_n(z_a)$ . In simple terms, the main difference with respect to the local case is that the material resistivity is no longer described by a constant. Rather, as soon as spatial nonlocality is considered, the material resistivity becomes a function of the wave vector parallel to the surface  $p$ . In analogy with the local description we define the nonlocal resistivity as  $\rho(p) \equiv \partial_\omega r_I^{\text{TM}}(\omega, p)|_{\omega=0} / (2\epsilon_0)$ . In principle, one could also define a resistivity connected to the transverse electric reflection coefficient. Since the TE-waves give a sub-leading contribution in the near field, we skipped this distinction in order to keep the notational complexity at bay. The TM-reflection coefficient, for the interface to an infinitely extended half space medium can be written as a function of the surface impedance, i.e.

$$r^{\text{TM}}(\omega, p) = \frac{1 - Z^{\text{TM}}/Z_0^{\text{TM}}}{1 + Z^{\text{TM}}/Z_0^{\text{TM}}}, \quad (14)$$

where  $Z_0^{\text{TM}}$  is the corresponding relation of the vacuum given by Eq. (1a) with  $\epsilon = 1$ . We obtain for the spatially

nonlocal resistivity

$$\rho(p) = \frac{2}{\pi\epsilon_0} \frac{\int_0^\infty dq \frac{p}{k^2} \text{Im} \left\{ \frac{\partial_\omega \epsilon_l(\omega, k)|_{\omega=0}}{[\epsilon_l(0, k)]^2} \right\}}{\left[ 1 + \frac{2}{\pi} \int_0^\infty dq \frac{p}{k^2 \epsilon_l(0, k)} \right]^2}. \quad (15)$$

In general, Eq. (15) depends on all the intrinsic length-scales characterizing the material. The most relevant ones for our analysis are the Thomas-Fermi screening length  $\lambda_{\text{TF}} = v_F/(\sqrt{3}\omega_p)$  and the mean free path  $\ell = v_F/\Gamma$ , with typical values between a few angstroms and a few tens of nanometers, respectively. Figure 1 shows the resistivity as a function of the wvector for the permittivities in Eq. (2) and Eq. (5). For the description based on the Boltzmann-Mermin model, the resistivity  $\rho(p)$  features a maximum around  $p \sim 1/(5\lambda_{\text{TF}})$ , where it can be more than an order of magnitude larger than its local counterpart,  $\rho_{\text{lc}} = \Gamma/(\epsilon_0\omega_p^2)$ . In the case of the hydrodynamic description with a frequency-dependent compressibility factor, the resistivity has instead a maximum for  $p \sim 1/(2\lambda_{\text{TF}})$  with a value that is  $\sim 2\omega_p^2/(5\Gamma^2)$  times larger than the value for the local description. At this point, we should like to note that the behavior of  $\beta(\omega)$  is essential for this result: The resistivity for the extended hydrodynamic model can indeed be written as the sum of two contributions

$$\rho_{\text{eH}}(p) = \rho_{\text{H}}(p) + \rho_{\text{Ld}}(p). \quad (16)$$

The expression  $\rho_{\text{H}}(p)$  is the resistivity one would have obtained for a constant value of  $\beta = \beta(0)$ , i.e. for the usual common hydrodynamic description, while  $\rho_{\text{Ld}}(p)$  is a correction due to the frequency dependence of the compressibility factor ( $\sim \partial_\omega \beta(\omega)|_{\omega=0}$ ). The first term is dominated by the collision-induced damping of quasi-particles in the conductor. It monotonously decreases from the value  $\rho_{\text{lc}}$  for  $p\lambda_{\text{TF}} \ll 1$  to zero for  $p\lambda_{\text{TF}} \gg 1$ . It is, therefore, the second contribution,  $\rho_{\text{Ld}}(p)$ , which dominates  $\rho_{\text{eH}}(p)$  in the nonlocal regime and gives rise to the aforementioned maximum. Due to its intrinsic connection to the frequency-dependence of the compressibility factor  $\beta(\omega)$ ,  $\rho_{\text{Ld}}(p)$  physically encodes the process of Landau damping. For very large wave vectors,  $p \gg \ell^{-1}$ , spatial dispersion becomes negligible and both the hydrodynamic and the Boltzmann-Mermin model (see Fig. 1 and Ref. [12]) approach the local Drude description. More detailed expressions can be found in the Appendix A. Inspecting the force in Eq. (9) and the definition of  $\mathcal{D}_n(z_a)$ , we can conclude that a *constant* compressibility factor in the (nonlocal) hydrodynamic description modifies the quantum frictional force relative to that with the local counterpart of the material model only for distances  $z_a \ll \lambda_{\text{TF}}$ . These are distances outside the range of validity of our theory. Conversely, if  $\beta = \beta(\omega)$ , modifications already occur for considerably larger atom-surface separations ( $z_a \sim \ell$ ). Figure 1 shows that, although the resistivity of the extended hydrodynamic model qualitatively resembles the Boltzmann-Mermin model, it quantitatively overestimates the impact of nonlocality.

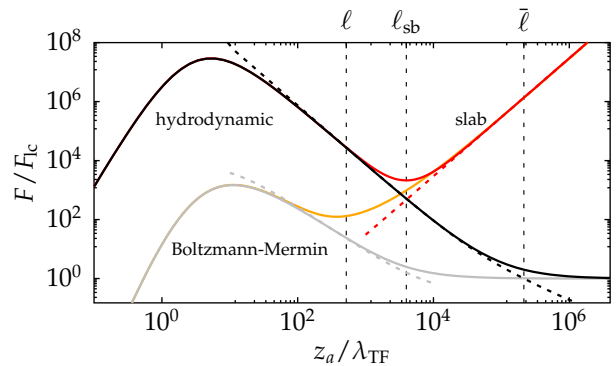


FIG. 2. Quantum frictional force experienced by an atom moving at low velocity parallel to a planar interface at separation  $z_a$  [Eq. (11)]. We normalize to the local Drude result  $F_{\text{lc}}$  (see Eq. (13) and Ref. [12]). The drag force near a semi-infinite bulk and a slab with thickness  $d = 10^2\lambda_{\text{TF}} \approx 9\text{nm}$  is depicted. The black (bulk) and the red (slab) lines corresponds to the permittivity given by the extended hydrodynamic model. The gray (bulk) and the orange (slab) lines refer instead to the Boltzmann-Mermin model. The asymptotes of Eqs. (17) and (24) as well as for the Boltzmann-Mermin model from Ref. [12] are given in dashed lines. Parameters are chosen as in Fig.1.

This behavior is reflected in the frictional force. Indeed, from Eq. (12b) we obtain that the dominant contributions to the force in the planar setup stem from wave vectors  $p \sim 1/(2z_a)$ . In accordance with the maxima of the corresponding resistivity (see Fig. 1), quantum friction thus features a maximum at  $z_a \sim 10\lambda_{\text{TF}}$  for the Boltzmann-Mermin description and a maximum at  $z_a \sim 4\lambda_{\text{TF}}$  for the hydrodynamic model. Further, both models predict an enhancement of several orders of magnitude for the frictional interaction. Again, despite the qualitative similarities in the behavior of the force, if the Boltzmann-Mermin description is taken as reference, the extended hydrodynamic model gives rise to a force which is several orders of magnitude larger (see Fig. 2). To be more concrete, we average over all dipole orientations in Eq. (11) and find that in the nonlocal regime ( $z_a \sim \ell$ )

$$\frac{F}{F_{\text{lc}}} \approx \frac{\omega_p^2}{\Gamma^2} \left( 2 \frac{\lambda_{\text{TF}}}{z_a} + \frac{73}{240} \frac{\ell^2}{z_a^2} \right). \quad (17)$$

For separations  $z_a \gg \bar{\ell} \approx 1.4 \frac{\omega_p}{\Gamma} \ell$ , Landau damping completely loses impact and the extended hydrodynamic description transitions into the regime dominated by spatially local (Drude) physics (see Appendix A). Employing the extended hydrodynamic description, the frictional force is still described by a power law, but as compared to the local model with a different exponent. In contrast, in Ref. [12] it was shown that the Boltzmann-Mermin model produces a logarithmic behavior. Still, the hydrodynamic model for conducting materials in the form suggested by Halevi offers an analytically much simpler structure whilst conserving the most important physical features. In this way, it becomes adequate for qualita-

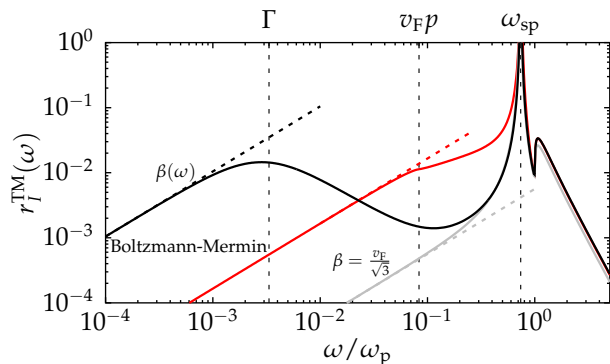


FIG. 3. Frequency dependence of the imaginary part of the TM reflection coefficient of a planar interface between vacuum and metal-filled half-space. The permittivity of the bulk is modeled using the Boltzmann-Mermin model (red), the extended hydrodynamic description (black) and standard hydrodynamic model (gray). The linear (Ohmic) regime is given in dashed lines. The parameters are chosen as in Fig. 1 and  $p = 50/(2\ell)$ . For these values the local (Drude) model (not shown) is almost identical to the standard hydrodynamic description.

tively studying more complicated geometries which we illustrate in the following section by considering the interaction with a planar slab (thin film) of metal. At this point, it is interesting to discuss the validity of the Ohmic approximation for the material models considered in our work (see Fig. 3). While all descriptions are essentially equivalent for frequencies larger or of the order of the surface plasmon-polariton resonance  $\omega_{\text{sp}}$  (see Ref. [48]), they are very different in the low frequency region. The Ohmic range, where the  $r_I^{\text{TM}} \propto \omega$ , is characteristic of each model. While for the local description and the standard hydrodynamic expression  $r_I^{\text{TM}} \propto \omega$  for  $\omega \ll \omega_{\text{sp}}$ , the Boltzmann-Mermin model as well as the extended hydrodynamic model feature additional length scales limiting the Ohmic approximation. The Boltzmann-Mermin model displays Ohmic behavior as long as the radiation's frequency dominating the interaction  $\omega$  is smaller than either the collision-rate  $\Gamma$  or than the value  $v_F p$ . In other words, the material is Ohmic as long as some damping mechanism (either collision-induced or Landau damping) is present. Note that both frequency scales are encoded in the parameter  $u$  [see its definition after Eqs. (3)]. In the extended hydrodynamic model with the Halevi correction, however, only one of the above frequency scales is present. Mathematically, this can be seen from the linear relation between the compressibility factor and the Fermi velocity  $\beta \propto v_F(\frac{3}{5}\omega + \frac{1}{3}\Gamma)/(\omega + i\Gamma)$ . Since  $v_F$  is constant, the only intrinsic frequency scale derives from the complex prefactor and is given by the dissipation rate  $\Gamma$ . For frequencies  $\omega \gg \Gamma$ , the model automatically approaches its high-frequency limit. Further, we want to comment on the range of validity of the asymptotic expression in Eq. (11) which is based on the Ohmic behavior of the reflection coefficient. Since the

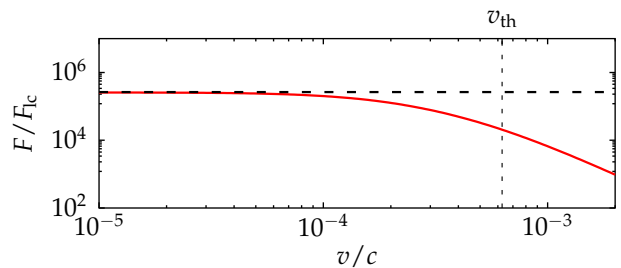


FIG. 4. Full retarded velocity dependence of the quantum frictional force using the extended hydrodynamic model for a half-space geometry. The force is normalized by the non-retarded Ohmic result obtained for the local Drude model [see after Eq. (13)] to highlight the deviation from the  $v^3$  behavior. The atom-surface separation was chosen to be  $z_a = 10 \text{ nm} \sim 10^2 \lambda_{\text{TF}}$ , where the standard hydrodynamic model with constant and real  $\beta$  and the local Drude model coincide. The parameters are chosen as in Fig. 1. The value  $v_{\text{th}}$  [see Eq. (18)] is an estimate for the breakdown of the Ohmic regime. The dashed horizontal line represents the Ohmic approximation of Eq. (17).

scaling of the reflection coefficient with frequency is intrinsically connected to the velocity scaling of the force [49], each model leads to a different velocity dependence of the frictional force above the Ohmic threshold. As a rough estimate of the threshold velocity  $v_{\text{th}}$  for the hydrodynamic model with frequency-dependent  $\beta$ , we compare its linear regime with the value of the reflection coefficient at its plateau, where  $\omega \sim \Gamma$  (see black curve in Fig. 3). This constraints the validity of the linear regime of the extended hydrodynamic model to frequencies  $\omega \lesssim r_I^{\text{TM}}(\Gamma, p)/(2\epsilon_0 \rho_{\text{eH}}(p))$  ( $p \ll \lambda_{\text{TF}}^{-1}$ ), where  $\rho_{\text{eH}}$  is the respective resistivity. Since the frictional force on atoms is dominated by frequencies  $\omega \lesssim \mathbf{p} \cdot \mathbf{v}$  and for the planar geometry we have that  $p \sim z_a^{-1}$  [46], we conclude that the Ohmic response of the extended hydrodynamic model holds for velocities (see Fig. 4)

$$v \ll v_{\text{th}} = \frac{z_a}{2\epsilon_0 \rho_{\text{eH}}} r_I^{\text{TM}}(\Gamma, z_a^{-1}). \quad (18)$$

Notice that, due to the integration over the frequency appearing in the definition of quantum friction, these features are smoothed out in the force, reducing these differences in the functional dependence on the velocity as can be seen in Fig. 4.

## B. Nonlocal thin films

One major (technical) inconvenience of the Boltzmann-Mermin model is its complexity which leads to rather involved mathematical expressions when going beyond the simple half-space geometry that we have considered so far. In fact, this already applies to slab geometries. Consequently, owing to their more

transparent mathematical expressions, we limit the following discussion of thin metal films to the extended hydrodynamic model. To contrast our findings, we report the numerical results for the Boltzmann-Mermin model and provide a physical interpretation in terms of the system's length scales. The description of a slab's reflection coefficients requires a non-trivial mathematical treatment when nonlocality is taken into account. The main reason is that the field in a spatially dispersive medium is not necessarily transverse and the distinction between transverse and longitudinal waves becomes important. For propagation along the  $z$ -direction (perpendicular to the surface) in bulk we can associate two field components, for example  $E_x$  and  $B_y$ , with the transverse propagation and the field component  $E_z$  and the scalar potential  $\phi$  with the longitudinal propagation. For planar geometries such as single- or multi-layered systems stacked in  $z$ -direction, the propagation can then be described using the transfer-matrix approach [50, 51]. For a nonlocal layer with thickness  $d$  this technique relates the fields at one interface ( $z = z_0$ ) to those on the opposite interface ( $z = z_0 + d$ ), i.e.

$$\begin{pmatrix} E_x \\ cB_y \\ E_z \\ \phi \end{pmatrix}_{z=z_0+d}^{\sigma} = \mathbb{Y}^{\sigma}(d) \begin{pmatrix} E_x \\ cB_y \\ E_z \\ \phi \end{pmatrix}_{z=z_0}^{\sigma}, \quad (19)$$

where  $\mathbb{Y}^{\sigma}(d)$  is a  $4 \times 4$  transfer matrix containing information about the propagation through the medium and  $\sigma$  indicates the different transverse polarizations TM and TE. At each interface, both longitudinal and transverse fields are then connected via ABCs [26, 27, 52–54]. The ABCs effectively reduce the four independent fields of Eq. (19) to the two transverse fields of the local material adjacent to the nonlocal slab of finite extent,

$$\begin{pmatrix} E_x \\ cB_y \end{pmatrix}_{z=z_0+d}^{\sigma} = \mathbb{M}^{\sigma}(d) \begin{pmatrix} E_x \\ cB_y \end{pmatrix}_{z=z_0}^{\sigma}. \quad (20)$$

The resulting  $2 \times 2$  transfer matrix is given by

$$\mathbb{M}^{\sigma}(d) = \begin{pmatrix} \text{cs}_{\text{nl}}^{\sigma}(d) & i\delta^{\sigma} \mathcal{Z}_{\text{right}}^{\sigma}(d) \\ i\delta^{\sigma} / \mathcal{Z}_{\text{left}}^{\sigma}(d) & \text{cs}_{\text{nl}}^{\sigma}(d) \end{pmatrix}, \quad (21)$$

where  $\delta^{\text{TM/TE}} = \pm 1$ , while  $\mathcal{Z}_{\text{left}}^{\sigma}(d)$ ,  $\mathcal{Z}_{\text{right}}^{\sigma}(d)$  and  $\text{cs}_{\text{nl}}^{\sigma}(d)$  are complex functions describing the propagation in the nonlocal medium and the interaction with the two interfaces that limit the nonlocal layer. Here, we refrain from displaying the resulting, rather lengthy expression of  $\text{cs}_{\text{nl}}^{\sigma}(d)$ ,  $\mathcal{Z}_{\text{left}}^{\sigma}(d)$  and  $\mathcal{Z}_{\text{right}}^{\sigma}(d)$ . Instead, we refer to the Appendix B and to previous works for their detailed description [55]. Applying this transfer-matrix approach, the TM-polarized reflection coefficient for a thin slab can be written as

$$r_{\text{slab}}^{\text{TM}} = \frac{(Z_0^{\text{TM}})^2 - \mathcal{Z}_{\text{right}}^{\text{TM}} \mathcal{Z}_{\text{left}}^{\text{TM}}}{(Z_0^{\text{TM}})^2 + \mathcal{Z}_{\text{right}}^{\text{TM}} \mathcal{Z}_{\text{left}}^{\text{TM}} + 2i \text{cs}_{\text{nl}}^{\text{TM}} Z_0^{\text{TM}} \mathcal{Z}_{\text{left}}^{\text{TM}}} \quad (22)$$

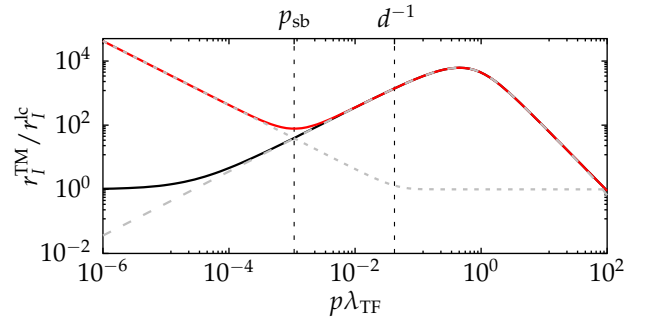


FIG. 5. Imaginary part of the TM-reflection coefficient normalized to the corresponding low-frequency Drude result,  $r_l^{\text{TM}} / r_l^c \approx 2\epsilon_0 \rho_{1c} \omega$ , as a function of the wave vector  $p$  for different geometries and given frequency  $\omega/\omega_p = 10^{-5}$  (Ohmic region). The slab's (red solid line) and the half-space's reflection coefficient (black solid line) feature a different behavior for small wave vectors  $p \ll p_{\text{sb}}$  [see Eq. (23) and below]. We report the corresponding asymptotic characteristics in gray (dashed line for  $\rho_{\text{Ld}}(p)$  and dotted line for  $\rho_{\text{H}}(p) \coth[dp]$ ). The parameters are the same as in Fig. 1 and we set the layer thickness to  $d = 1 \text{ nm} \sim 10\lambda_{\text{TF}}$ .

where, in order to shorten the notation, we have dropped the explicit  $d$ -dependence. In Fig. 5 we depict the imaginary part of the reflection coefficient in Eq. (22) as a function of the wave vector  $p$  and compare it to the corresponding result of a half-space geometry [see Eq. (14)]. The graph highlights how in the slab geometry the behavior for small wavevectors is altered due to the occurrence of the additional geometric length scale  $d$ . At low frequencies, for values  $p \ll \lambda_{\text{TF}}^{-1}$  where the material exhibits nonlocal behavior, the imaginary part of the reflection coefficient in Eq. (22) is related to the slab resistivity

$$\rho_{\text{sb}}(p) = \rho_{\text{H}}(p) \coth[dp] + \rho_{\text{Ld}}(p). \quad (23)$$

Equation (23) generalizes the expression for the resistivity in Eq. (16) to the slab geometry. The two contributions are depicted as gray lines in Fig. 5. As already shown in Sec. III A, the Landau damping dominates the hydrodynamic resistivity for wave vectors  $p \gtrsim \ell^{-1}$ . However, for  $p \ll 1/d$  the collision-induced contribution experiences an enhancement via the  $\coth[dp]$  factor. The enhancement of the collision-induced damping in the slab geometry relative to the half-space geometry can be understood by the symmetric coupling of the two surface plasmon-polaritons (SPPs) [56–58] at the two surfaces and has already been discussed for local materials in [49]. The transition wave vector, for which the contribution of the enhanced collision-induced and Landau damping exchange their role, is now given by  $p_{\text{sb}} \approx \sqrt{\frac{2}{5}}(\omega_p/\Gamma)\sqrt{d\lambda_{\text{TF}}}$  and can be obtained by equating the expressions of the corresponding resistivities [see Eq. (23)]. In Fig. 2, we depict the quantum frictional force on an atom moving above a thin nonlocal slab. For distances  $d \ll z_a \ll \ell$ , Eq. (17) is modified with respect

to the half-space results, i.e.

$$\frac{F}{F_{\text{lc}}} \approx \frac{227}{768} \frac{z_a^2}{d^2} + \frac{\omega_p^2}{\Gamma^2} \frac{73}{240} \frac{\ell^2}{z_a^2}. \quad (24)$$

The first term coincides with the force expected of a local Drude slab (see Ref. [49]). It dominates for separations  $z_a \gtrsim \ell_{\text{sb}} \approx 0.77\ell\sqrt{d/\lambda_{\text{TF}}} \sim p_{\text{sb}}^{-1}$ , where the interaction can resolve the structural details, i.e., the finite spatial extension  $d$  and the SPP coupling comes into play. The latter enhances the contribution of collision-induced damping and makes the corresponding force less sensitive to changes in the atom-surface separation [49]. Hence, this process dominates for large distances such that the physics is sufficiently described by the local Drude model. The situation changes when the atom approaches the surface: The second term of Eq. (24) is identically the result of Eq. (17) and corresponds to a bulk response dominated by Landau damping. Below  $\ell_{\text{sb}}$ , the interaction characterized by wavelengths  $\lambda \lesssim z_a$  cannot resolve the full geometry of the slab and perceives the surface as an infinitely extended bulk. For comparison, we report the numerical evaluation of the frictional force using the more involved Boltzmann-Mermin model (see Fig. 2). Noteworthy, the Boltzmann-Mermin model qualitatively and for larger separations (in the near-field description) also quantitatively confirms the findings we already obtained with the extended hydrodynamic description. Since the electron's mean free path that defines the regime of non-locality,  $\ell$ , is shorter than the length scale characterizing the transition from bulk to slab physics,  $\ell_{\text{sb}}$ , the model automatically approaches its local limit for separations  $z_a \gtrsim \ell_{\text{sb}}$ . Consequently, for the chosen material and geometry, the effects of spatial nonlocality play a sub-leading role as soon as the physics of quantum friction is dominated by the finite slab geometry.

#### IV. CONCLUSION AND DISCUSSIONS

In the present work, we have analyzed the drag force experienced by a moving atom interacting with a spatially dispersive conductor. We have placed special emphasis on the modeling of the conductor's low-frequency behavior and have compared an extended hydrodynamic description put forward by Halevi [19] to the rather involved Boltzmann-Mermin model [12]. The extended hydrodynamic description incorporates a complex-valued frequency-dependent compressibility factor of the Fermi fluid which can be deduced from an expansion of the Boltzmann-Mermin model for weak spatial nonlocality. Although much simpler than the Boltzmann-Mermin model, the extended hydrodynamic description does include dissipative energy transfer mechanisms in terms of Landau damping and thus sharply contrasts to the standard hydrodynamic approaches that utilize real-valued and frequency-independent compressibility factor. The extended hydrodynamic model is, therefore, well-suited

to qualitatively investigate the impact of nonlocal damping mechanisms on geometrically and/or dynamically complex quantum-optical setups.

We have illustrated this by computing quantum friction forces for both, infinite half-spaces and thin metallic slabs. In the half-space geometry, we have shown that the extended hydrodynamic model essentially contains the enhancement of the force with respect to a local Drude description predicted by the Boltzmann-Mermin model for atom-surface separations of the order of the bulk electron's mean free path. This result is related to Landau damping and is not present in the standard hydrodynamic description. However, the extended hydrodynamic description overestimates the enhancement by several orders of magnitude with respect to the more fundamental Boltzmann-Mermin model. On the other hand, for the slab geometry the extended hydrodynamic description has proved to be very practical in order to gain reliable insights into the interplay of the different physical damping processes: For atom-surface separations smaller than  $\ell_{\text{sb}}$ , a characteristic length scale connected to the slab's thickness and the internal damping mechanisms of the material (see Sec. III B), the interaction is insensitive to the slab's finite thickness, resulting in a frictional force which equals that obtained for the half-space geometry. For larger separations, however, the interaction involves the surface-plasmon polaritons which couple across the slab. The finite thickness of the slab appreciably influences their behavior and the frictional force experiences a modification in its functional dependence on the atom-surface separation. Interestingly, as long as the slab thickness is not much smaller than the mean free path, the impact of spatial nonlocality in the extended hydrodynamic description becomes negligible and the force coincides with the result using a local Drude description of the material. This phenomenon is connected to the distinct natures of collision-induced and Landau damping, respectively. Collision-induced damping describes a multi-scattering average of the quasi-particles in the Fermi liquid with respect to the wavelength of the electromagnetic mode, which is also available in spatially local material models independent of the radiation's wave vector. Landau damping is intrinsically connected to the spatial correlation in the system and thereby couples non-trivially to the length scales of the slab geometry. In the slab geometry, the impact of the latter turns out to be more constrained with respect to the half-space geometry.

The standard hydrodynamic model has become popular in describing the nonlocal optical response of nanophotonic systems [59, 60]. Commonly, one has to solve Maxwell's equations in non-trivial geometries and relies here on sophisticated numerical solvers (see e.g. Ref. [61] for a method in the time-domain), where material descriptions are included by means of partial differential equations for macroscopic electrodynamic quantities fulfilling additional boundary conditions [60]. Including descriptions as complex as the Boltzmann-Mermin model

is, therefore, numerically a highly non-trivial problem (especially for non-planar geometries) and researchers are pushing towards extensions of the hydrodynamic equations [20, 32]. Our analyses delineates the limits of applicability of the aforementioned material models in the context of nonequilibrium fluctuation-induced interactions and provides a transparent physical interpretation of the roles of collision-induced and Landau damping. In view of the serious challenges related to a numerical implementation of the more fundamental Boltzmann-Mermin model and the relative ease of implementing the standard hydrodynamic model, our work is also of relevance for further investigations regarding extensions of the hydrodynamic description. An example is provided by the analysis of Casimir(-Polder) forces in systems involving spatially nonlocal material and non-trivial geometries beyond the analytically accessible cases. [62, 63].

### ACKNOWLEDGEMENTS

We thank D. Huynh for fruitful discussions. We acknowledge support from the Deutsche Forschungsgemeinschaft (DFG) through the DIP program (Grant No. SCHM 1049/7-1) and the DFG Collaborative Research Center (CRC) 951 Hybrid Inorganic/ Organic Systems for Opto- Electronics (Project B10).

#### Appendix A: Resistivity and friction using the hydrodynamic model

In this Appendix, we derive the expression for the resistivity of the hydrodynamic material model, Eqs. (15) and (16), and deduce the quantum frictional force experienced by an atom in motion relative to a material-filled half-space as reported in Eq. (17). Starting from Eq. (1a) and inserting the relation for the permittivities given by Eq. (5), we obtain for the TM surface impedance of the hydrodynamic model

$$\frac{Z_0^{\text{TM}}}{Z_0^{\text{TM}}} = \frac{1}{\epsilon_{\text{Dr}} \kappa} \left( \kappa_\epsilon + \frac{p(\epsilon_{\text{Dr}} - 1)}{\sqrt{1 + \frac{\omega_p^2}{\beta^2 p^2} \frac{\epsilon_{\text{Dr}}}{\epsilon_{\text{Dr}} - 1}}} \right), \quad (\text{A1})$$

where we have defined  $\kappa = \sqrt{p^2 - \omega^2/c^2}$  and  $\kappa_\epsilon = \sqrt{p^2 - \epsilon_{\text{Dr}} \omega^2/c^2}$  with  $\text{Im} \kappa, \text{Im} \kappa_\epsilon < 0$ . In the near-field regime (formally  $c \rightarrow \infty$ ), the TM reflection coefficient reduces to

$$r^{\text{TM}} = \frac{\epsilon_{\text{Dr}} - 1}{\epsilon_{\text{Dr}} + 1 + 2(\epsilon_{\text{Dr}} - 1) \frac{\beta^2 p^2}{\omega_p^2} \left( 1 + \sqrt{1 + \frac{\omega_p^2}{\beta^2 p^2} \frac{\epsilon_{\text{Dr}}}{\epsilon_{\text{Dr}} - 1}} \right)}. \quad (\text{A2})$$

In the limit of vanishing spatial dispersion (formally  $\beta \rightarrow 0$ ), this last result reduces to the usual local expression  $r^{\text{TM}} \rightarrow (\epsilon_{\text{Dr}} - 1)/(\epsilon_{\text{Dr}} + 1)$ . For frequencies

$\omega \ll \Gamma$ , using the frequency dependent compressibility factor  $\beta(\omega)$  given in Eq. (7) the reflection coefficient behaves Ohmic (see main text), i.e.

$$r^{\text{TM}} \approx R(\lambda_{\text{TFP}}) + 2i\epsilon_0 \rho_{\text{eH}}(\lambda_{\text{TFP}})\omega, \quad (\text{A3})$$

where we have defined the real function

$$R(x) = 1 + 2x \left( x - \sqrt{1 + x^2} \right) \rightarrow \begin{cases} 1, & x \ll 1 \\ (2x)^{-2}, & x \gg 1 \end{cases}, \quad (\text{A4})$$

which corresponds to the reflection coefficient for  $\omega = 0$  and exhibits an absolute value that is smaller or equal to one. Further, the resistivity decomposes into a sum of two terms,  $\rho_{\text{eH}}(\lambda_{\text{TFP}}) = \rho_{\text{H}}(\lambda_{\text{TFP}}) + \rho_{\text{Ld}}(\lambda_{\text{TFP}})$ , associated with distinct damping mechanisms. The first one is connected to collision-induced damping of quasi-particles in the Fermi liquid,

$$\rho_{\text{H}}(x) = \frac{\Gamma}{\epsilon_0 \omega_p^2} \frac{\frac{x}{2} (\sqrt{x^2 + 1} + 2x) + 1}{(x^2 + 1) (2x (\sqrt{x^2 + 1} + x) + 1)^2} \rightarrow \frac{\Gamma}{\epsilon_0 \omega_p^2} \begin{cases} 1, & x \ll 1 \\ \frac{3}{32x^2} \frac{1}{2+x^2}, & x \gg 1 \end{cases} \quad (\text{A5})$$

and the other is connected to Landau damping in the bulk,

$$\rho_{\text{Ld}}(x) = \frac{i}{\epsilon_0} \frac{\beta'(0)}{\beta(0)} \frac{x (2x^2 (\sqrt{x^2 + 1} + x) + \sqrt{x^2 + 1} + 2x)}{(x^2 + 1) (2x (\sqrt{x^2 + 1} + x) + 1)^2} \rightarrow \frac{i}{\epsilon_0} \frac{\beta'(0)}{\beta(0)} \begin{cases} x, & x \ll 1 \\ \frac{1}{4} \frac{1}{1+x^2}, & x \gg 1 \end{cases}. \quad (\text{A6})$$

Here, the prime denotes the derivative with respect to frequency. This second term only appear for a complex-valued and frequency-dependent compressibility factor  $\beta(\omega)$  and in the main text this was associated with a resistivity originating from Landau damping. Models with real-valued  $\beta$  only feature the collision-induced resistivity  $\rho_{\text{H}}$ . Further, while both  $R(x)$  and  $\rho_{\text{H}}$  are monotonously decreasing functions of  $x$ ,  $\rho_{\text{Ld}}(x)$  first monotonously increases, then exhibits a maximum at  $x = \sqrt{\sqrt{2}^{-1} - 2^{-1}} \approx 0.46$ , and finally monotonously approaches zero for increasing  $x$ . This behavior becomes apparent in Fig. 1. From Eq. (11), we infer that the low-velocity quantum frictional force is given in terms of the function  $\mathcal{D}_n(z_a)$  with  $n = 0, 1, 2$ . Since the latter is a linear functional of the resistivity, it also decomposes into two contributions related to collision-induced and Landau damping, respectively. In particular, we have

$$\mathcal{D}_n^{\text{eH}}(z_a) = \mathcal{D}_n^{\text{H}}(z_a) + \mathcal{D}_n^{\text{Ld}}(z_a), \quad (\text{A7})$$

which can be evaluated exactly for the limiting cases of small and large  $x = p\lambda_{\text{TF}}$ , respectively, yielding

$$\mathcal{D}_{\{0,1,2\}}^{\text{H}} \quad (\text{A8a})$$

$$\rightarrow 2\epsilon_0\rho_{\text{lc}} \begin{cases} \left\{ \frac{3\pi}{64\sqrt{2}\lambda_{\text{TF}}^3}, \frac{1}{z_a} \frac{3}{64\lambda_{\text{TF}}^4}, \frac{1}{z_a^3} \frac{3}{128\lambda_{\text{TF}}^4} \right\}, & z_a \ll \lambda_{\text{TF}} \\ \left\{ \frac{1}{4z_a^3}, \frac{3}{4z_a^5}, \frac{45}{8z_a^7} \right\}, & z_a \gg \lambda_{\text{TF}} \end{cases}$$

$$\mathcal{D}_{\{0,1,2\}}^{\text{Ld}} \quad (\text{A8b})$$

$$\rightarrow \frac{4}{5\Gamma} \begin{cases} \left\{ \frac{1}{z_a} \frac{1}{8\lambda_{\text{TF}}^2}, \frac{1}{z_a^3} \frac{1}{16\lambda_{\text{TF}}^2}, \frac{1}{z_a^5} \frac{3}{16\lambda_{\text{TF}}^2} \right\}, & z_a \ll \lambda_{\text{TF}} \\ \left\{ \frac{1}{z_a^4} \frac{3\lambda_{\text{TF}}}{8}, \frac{1}{z_a^6} \frac{15\lambda_{\text{TF}}}{8}, \frac{1}{z_a^8} \frac{315\lambda_{\text{TF}}}{16} \right\}, & z_a \gg \lambda_{\text{TF}} \end{cases}$$

Here, we have introduced the abbreviation  $\rho_{\text{lc}} = \Gamma/(\epsilon_0\omega_{\text{p}}^2)$  and have used that  $i\beta'(0)/(\epsilon_0\beta(0)) = 2/(5\epsilon_0\Gamma)$ . For typical metals, the Thomas-Fermi screening length  $\lambda_{\text{TF}}$  lies in the range of a few angstroms, a range for that our theory is not valid anymore. Hence, for all practical cases, we have the situation that  $z_a \gg \lambda_{\text{TF}}$  and the second set of lines of Eqs. (A8) apply. This means that  $\mathcal{D}_n^{\text{H}} \approx \mathcal{D}_n^{\text{lc}}$  reduces to the local Drude result  $\mathcal{D}_n^{\text{lc}}$  reported in Ref. [46] and we obtain for the quantum frictional force experienced by an atom in the half-space geometry

$$\begin{aligned} \frac{F}{F_{\text{lc}}} - 1 &\approx \frac{\frac{\Phi_0\Phi_2}{3} (\mathcal{D}_0^{\text{lc}}\mathcal{D}_2^{\text{Ld}} + \mathcal{D}_0^{\text{Ld}}\mathcal{D}_2^{\text{lc}} + \mathcal{D}_0^{\text{Ld}}\mathcal{D}_2^{\text{Ld}})}{\frac{\Phi_0\Phi_2}{3}\mathcal{D}_0^{\text{lc}}\mathcal{D}_2^{\text{lc}} + \Phi_1^2 [\mathcal{D}_1^{\text{lc}}]^2} \\ &+ \frac{\Phi_1^2 (2\mathcal{D}_1^{\text{lc}}\mathcal{D}_1^{\text{Ld}} + [\mathcal{D}_1^{\text{Ld}}]^2)}{\frac{\Phi_0\Phi_2}{3}\mathcal{D}_0^{\text{lc}}\mathcal{D}_2^{\text{lc}} + \Phi_1^2 [\mathcal{D}_1^{\text{lc}}]^2}, \end{aligned} \quad (\text{A9})$$

where  $F_{\text{lc}}$  is the local Drude result (see main text). Expressing the atomic dipole moment  $\mathbf{d}$  in polar coordinates and averaging over all possible directions, we obtain

$$\left\langle \frac{\Phi_0\Phi_2}{3} \right\rangle = \frac{7}{7680\pi^2} \frac{\alpha_0^2}{\epsilon_0^2} \quad \langle \Phi_1^2 \rangle = \frac{29}{15360\pi^2} \frac{\alpha_0^2}{\epsilon_0^2} \quad (\text{A10})$$

where  $\alpha_0 = \sum_i \alpha_{ii}/3$ . This leads to

$$\frac{F}{F_{\text{lc}}} \approx 1 + \frac{\omega_{\text{p}}^2}{\Gamma^2} \left( 2 \frac{\lambda_{\text{TF}}}{z_a} + \frac{73}{240} \frac{\ell^2}{z_a^2} \right). \quad (\text{A11})$$

Noticing that the second term is dominant in the nonlocal regime, the expression restores the relation reported in Eq. (17). From the previous equation, we conclude that the frictional force using the extended hydrodynamic model differs substantially from the local Drude result  $F_{\text{lc}}$  for separations

$$z_a \ll \bar{\ell} := \left( \frac{1}{\sqrt{3}} + \frac{1}{4} \sqrt{\frac{51}{5}} \right) \frac{\omega_{\text{p}} \ell}{\Gamma} \approx 1.4 \frac{\omega_{\text{p}} \ell}{\Gamma}. \quad (\text{A12})$$

This has been confirmed by numerical evaluation (see Fig. 2).

## Appendix B: Transfer-Matrix Approach using the hydrodynamic model

As discussed in Sec. III B, without ABCs the hydrodynamic model yields four linearly independent variables ( $E_x, cB_y, E_z, \phi$ ) [27]. In the transfer-matrix approach, the propagation of those fields through a single hydrodynamic slab is written in terms of a  $4 \times 4$  matrix  $\mathbb{Y}(d)^\sigma$  with respect to these four variables [see Eq. (19)]. This matrix,

$$\mathbb{Y}(d)^\sigma = Z_{\text{H}}^\sigma \mathbb{P}_{\text{H}}(d) (Z_{\text{H}}^\sigma)^{-1}, \quad (\text{B1})$$

is composed of a propagation matrix of left- and right-propagating transverse and longitudinal fields

$$\mathbb{P}_{\text{H}}(d) = \text{diag} [e^{iq_t d}, e^{-iq_t d}, e^{iq_l d}, e^{-iq_l d}], \quad (\text{B2})$$

where  $q_t/l$  are implicitly defined via

$$\epsilon_t(\omega)\omega^2 = (p^2 + q_t^2)c^2 \quad \text{and} \quad \epsilon_l(\omega, \sqrt{p^2 + q_l^2}) = 0, \quad (\text{B3})$$

which is ‘‘sandwiched’’ between two surface impedance matrices at the respective interfaces. In fact, owing to the symmetry of the system, one of the interface matrices is the inverse of the other [as anticipated in Eq. (B1)]. Explicitly, the interface matrix reads

$$Z_{\text{H}}^\sigma = -\frac{1}{2\epsilon_0 c} \begin{pmatrix} Z_{\text{Dr}}^\sigma & Z_{\text{Dr}}^\sigma & ik & ik \\ 1 & -1 & 0 & 0 \\ -W_{\text{Dr}} & W_{\text{Dr}} & iq_l & -iq_l \\ 0 & 0 & -1 & -1 \end{pmatrix}, \quad (\text{B4})$$

with

$$Z_{\text{Dr}}^{\text{TM}} = \frac{cq_t}{\omega\epsilon_{\text{Dr}}(\omega)}, \quad Z_{\text{Dr}}^{\text{TE}} = \frac{\omega}{cq_t}, \quad W_{\text{Dr}} = \frac{ck}{\omega\epsilon_{\text{Dr}}(\omega)}. \quad (\text{B5})$$

However, if we apply the ABCs at the interfaces, we match the fields of the nonlocal material with the fields of the adjacent local material and thus obtain the reduced  $2 \times 2$  transfer matrix for local materials, as written in Eq. (21) of the Sec. III B. This matrix relates to  $\mathbb{Y}$  of Eq. (B1) as follows

$$\mathbb{M}_{11} = \mathbb{Y}_{11} - \mathbb{Y}_{14} \frac{W_0 \mathbb{Y}_{21} + \mathbb{Y}_{31}}{W_0 \mathbb{Y}_{24} + \mathbb{Y}_{34}} \quad (\text{B6})$$

$$\mathbb{M}_{12} = \mathbb{Y}_{12} - W_0 \mathbb{Y}_{13} - \mathbb{Y}_{14} \left( \frac{W_0 \mathbb{Y}_{22} + \mathbb{Y}_{32}}{W_0 \mathbb{Y}_{24} + \mathbb{Y}_{34}} - W_0 \frac{W_0 \mathbb{Y}_{23} + \mathbb{Y}_{33}}{W_0 \mathbb{Y}_{24} + \mathbb{Y}_{34}} \right)$$

$$\mathbb{M}_{21} = \mathbb{Y}_{21} - \mathbb{Y}_{24} \frac{W_0 \mathbb{Y}_{21} + \mathbb{Y}_{31}}{W_0 \mathbb{Y}_{24} + \mathbb{Y}_{34}}$$

$$\mathbb{M}_{22} = \mathbb{Y}_{22} - W_0 \mathbb{Y}_{23} - \mathbb{Y}_{24} \left( \frac{W_0 \mathbb{Y}_{22} + \mathbb{Y}_{32}}{W_0 \mathbb{Y}_{24} + \mathbb{Y}_{34}} - W_0 \frac{W_0 \mathbb{Y}_{23} + \mathbb{Y}_{33}}{W_0 \mathbb{Y}_{24} + \mathbb{Y}_{34}} \right),$$

where  $W_0 = \frac{ck}{\omega}$ . In the previous equation, we have dropped the polarization index  $\sigma$ . For further details, we refer to Ref. [55].

- 
- [1] H. B. G. Casimir, On the attraction between two perfectly conducting plates, Proc. K. Ned. Akad. Wet. **51**, 793 (1948).
- [2] J. B. Pendry, Shearing the vacuum - quantum friction, J. Phys. Condens. Matter **9**, 10301 (1997).
- [3] G. Dedkov and A. Kyasov, Electromagnetic and fluctuation-electromagnetic forces of interaction of moving particles and nanoprobe with surfaces: A nonrelativistic consideration, Phys. Solid State **44**, 1809 (2002).
- [4] S. Scheel and S. Y. Buhmann, Casimir-Polder forces on moving atoms, Phys. Rev. A **80**, 042902 (2009).
- [5] V. Despoja, P. M. Echenique, and M. Šunjić, Nonlocal microscopic theory of quantum friction between parallel metallic slabs, Phys. Rev. B **83**, 205424 (2011).
- [6] A. I. Volokitin and B. N. J. Persson, Quantum Friction, Phys. Rev. Lett. **106**, 094502 (2011).
- [7] M. G. Silveirinha and S. I. Maslovski, Exchange of momentum between moving matter induced by the zero-point fluctuations of the electromagnetic field, Phys. Rev. A **86**, 042118 (2012).
- [8] M. Belén Farías, C. D. Fosco, F. C. Lombardo, F. D. Mazzitelli, and A. E. Rubio López, Functional approach to quantum friction: Effective action and dissipative force, Phys. Rev. D **91**, 105020 (2015).
- [9] A. I. Volokitin and B. N. J. Persson, Near-field radiative heat transfer and noncontact friction, Rev. Mod. Phys. **79**, 1291 (2007).
- [10] G. V. Dedkov and A. A. Kyasov, Fluctuation-electromagnetic interaction under dynamic and thermal nonequilibrium conditions, Physics-Uspekhi **60**, 559 (2017).
- [11] A. I. Volokitin and B. N. J. Persson, Noncontact friction between nanostructures, Phys. Rev. B **68**, 155420 (2003).
- [12] D. Reiche, D. A. R. Dalvit, K. Busch, and F. Intravaia, Spatial dispersion in atom-surface quantum friction, Phys. Rev. B **95**, 155448 (2017).
- [13] L. D. Landau, On the vibrations of the electronic plasma, J. Phys. (USSR) **10**, 25 (1946), [Zh. Eksp. Teor. Fiz.16,574(1946)].
- [14] J. Jackson, *Classical Electrodynamics* (John Wiley and Sons Inc., New York, 1975).
- [15] G. W. Ford and W. H. Weber, Electromagnetic interactions of molecules with metal surfaces, Phys. Rep. **113**, 195 (1984).
- [16] J. Lindhard, On the properties of a gas of charged particles, Kgl. Danske Videnskab. Selskab Mat.-Fys. Medd. **28**, 1 (1954).
- [17] N. D. Mermin, Lindhard Dielectric Function in the Relaxation-Time Approximation, Phys. Rev. B **1-57**, 2362 (1970).
- [18] P.-O. Chapuis, S. Volz, C. Henkel, K. Joulain, and J.-J. Greffet, Effects of spatial dispersion in near-field radiative heat transfer between two parallel metallic surfaces, Phys. Rev. B **77**, 035431 (2008).
- [19] P. Halevi, Hydrodynamic model for the degenerate free-electron gas: Generalization to arbitrary frequencies, Phys. Rev. B **51**, 7497 (1995).
- [20] N. A. Mortensen, S. Raza, M. Wubs, T. Søndergaard, and S. I. Bozhevolnyi, A generalized non-local optical response theory for plasmonic nanostructures, Nat. Commun. **5**, 3809 EP (2014).
- [21] G. Toscano, J. Straubel, A. Kwiatkowski, C. Rockstuhl, F. Evers, H. Xu, N. Asger Mortensen, and M. Wubs, Resonance shifts and spill-out effects in self-consistent hydrodynamic nanoplasmonics, Nat. Commun. **6**, 7132 EP (2015).
- [22] M. Moferdt, T. Kiel, T. Sproll, F. Intravaia, and K. Busch, Plasmonic modes in nanowire dimers: A study based on the hydrodynamic Drude model including non-local and nonlinear effects, Phys. Rev. B **97**, 075431 (2018).
- [23] F. Bloch, Inkohärente Röntgenstreuung und Dichteschwankungen eines entarteten Fermigases, Helv. Phys. Acta **7**, 385 (1934).
- [24] K. L. Kliever and R. Fuchs, Anomalous Skin Effect for Specular Electron Scattering and Optical Experiments at Non-Normal Angles of Incidence, Phys. Rev. **172**, 607 (1968).
- [25] W. E. Jones, K. L. Kliever, and R. Fuchs, Nonlocal Theory of the Optical Properties of Thin Metallic Films, Phys. Rev. **178**, 1201 (1969).
- [26] P. J. Feibelman, Surface electromagnetic fields, Prog. Surf. Sci. **12**, 287 (1982).
- [27] W. L. Mochán, R. Fuchs, and R. G. Barrera, Surface contribution to the optical properties of nonlocal systems, Phys. Rev. B **27**, 771 (1983).
- [28] R. Esquivel, C. Villarreal, and W. L. Mochan, Exact surface impedance formulation of the Casimir force: Application to spatially dispersive metals, Phys. Rev. A **68**, 052103 (2003).
- [29] R. Esquivel-Sirvent, C. Villarreal, W. L. Mochan, A. M. Contreras-Reyes, and V. B. Svetovoy, Spatial dispersion in Casimir forces: a brief review, J. Phys. A Math. Gen. **39**, 6323 (2006).
- [30] B. Horovitz and C. Henkel, Surface plasmons at composite surfaces with diffusive charges, Europhys. Lett. **97**, 57010 (2012).
- [31] T. V. Teperik, P. Nordlander, J. Aizpurua, and A. G. Borisov, Robust Subnanometric Plasmon Ruler by Rescaling of the Nonlocal Optical Response, Phys. Rev. Lett. **110**, 263901 (2013).
- [32] S. Raza, S. I. Bozhevolnyi, M. Wubs, and N. A. Mortensen, Nonlocal Optical Response in Metallic Nanostructures, Journal of Physics: Condensed Matter **27**, 183204 (2015).
- [33] R. Schmidt and S. Scheel, Radiative heat transfer between spatially nonlocally responding dielectric objects, Journal of Physics B: Atomic, Molecular and Optical Physics **51**, 044003 (2018).
- [34] F. Bloch, Zum elektrischen Widerstandsgesetz bei tiefen Temperaturen, Zeitschrift für Physik **59**, 208 (1930).
- [35] E. Grneisen, Die Abhängigkeit des elektrischen Widerstandes reiner Metalle von der Temperatur, Annalen der Physik **408**, 530 (1933).
- [36] J. Bass, W. P. Pratt, and P. A. Schroeder, The temperature-dependent electrical resistivities of the alkali metals, Rev. Mod. Phys. **62**, 645 (1990).
- [37] In the idealized case of a perfect crystal, collision-induced damping approaches zero with vanishing temperature (see Ref. [64] for a recent discussion). This phenomenon generated discussions about the behavior of the equilibrium Casimir interaction and its thermodynamical con-

- sistency (see Refs. [65, 66] and [63] for recent treatments in the context of Casimir and Casimir-Polder interactions, respectively). However, in the present description of quantum friction, the impact of the transverse electric reflection coefficient turns out subleading especially at short atom-surface separations (near-fied limit) [43].
- [38] D.-N. Huynh, Ph.D. thesis, Humboldt-Universität zu Berlin, Mathematisch-Naturwissenschaftliche Fakultät, 2018.
- [39] C. Kittel, *Introduction to Solid State Physics*, 7th ed. (John Wiley and Son Inc., New York, 1996).
- [40] G. Barton, Some surface effects in the hydrodynamic model of metals, *Rep. Prog. Phys.* **42**, 963 (1979).
- [41] G. S. Atwal and N. W. Ashcroft, Relaxation of an electron system: Conserving approximation, *Phys. Rev. B* **65**, 115109 (2002).
- [42] A. I. Volokitin and B. N. J. Persson, Dissipative van der Waals interaction between a small particle and a metal surface, *Phys. Rev. B* **65**, 115419 (2002).
- [43] F. Intravaia, R. O. Behunin, C. Henkel, K. Busch, and D. A. R. Dalvit, Failure of Local Thermal Equilibrium in Quantum Friction, *Phys. Rev. Lett.* **117**, 100402 (2016).
- [44] F. Intravaia, R. O. Behunin, and D. A. R. Dalvit, Quantum friction and fluctuation theorems, *Phys. Rev. A* **89**, 050101(R) (2014).
- [45] J. M. Wylie and J. E. Sipe, Quantum electrodynamics near an interface, *Phys. Rev. A* **30**, 1185 (1984).
- [46] F. Intravaia, R. O. Behunin, C. Henkel, K. Busch, and D. A. R. Dalvit, Non-Markovianity in atom-surface dispersion forces, *Phys. Rev. A* **94**, 042114 (2016).
- [47] D. Barchiesi and T. Groszes, Fitting the Optical Constants of Gold, Silver, Chromium, Titanium, and Aluminum in the Visible Bandwidth, *Journal of Nanophotonics* **8**, 083097 (2014).
- [48] J. M. Pitarke, V. M. Silkin, E. V. Chulkov, and P. M. Echenique, Theory of surface plasmons and surface-plasmon polaritons, *Reports on Progress in Physics* **70**, 1 (2007).
- [49] M. Oelschläger, K. Busch, and F. Intravaia, Nonequilibrium Atom-Surface Interaction with Lossy Multilayer Structures, *Physical Review A* **97**, 062507 (2018).
- [50] P. Yeh, A. Yariv, and C.-S. Hong, Electromagnetic Propagation in Periodic Stratified Media. I. General Theory\*, *JOSA* **67**, 423 (1977).
- [51] A. Yariv and P. Yeh, *Optical Waves in Crystals: Propagation and Control of Laser Radiation*, *Wiley Series in Pure and Applied Optics* (Wiley, New York, 1984).
- [52] P. Halevi and R. Fuchs, Generalised Additional Boundary Condition for Non-Local Dielectrics. I. Reflectivity, *Journal of Physics C: Solid State Physics* **17**, 3869 (1984).
- [53] P. Halevi and G. Hernández-Cocoletzi, Additional Boundary Conditions: Critical Comparison between Theory and Experiment, *Physical Review Letters* **48**, 1500 (1982).
- [54] S. Pekar, The Theory of Electromagnetic Waves in a Crystal in Which Excitons Are Produced, *Soviet Physics JETP-USSR* **6**, 785 (1958).
- [55] F. Intravaia and K. Busch, Fluorescence in Nonlocal Dissipative Periodic Structures, *Phys. Rev. A* **91**, 053836 (2015).
- [56] A. Eguiluz, Density Response Function and the Dynamic Structure Factor of Thin Metal Films: Nonlocal Effects, *Physical Review B* **19**, 1689 (1979).
- [57] M. Fukui, V. C. Y. So, and R. Normandin, Lifetimes of Surface Plasmons in Thin Silver Films, *Phys. Stat. Sol. (B)* **91**, K61 (1979).
- [58] R. E. Camley and D. L. Mills, Collective Excitations of Semi-Infinite Superlattice Structures: Surface Plasmons, Bulk Plasmons, and the Electron-Energy-Loss Spectrum, *Phys. Rev. B* **29**, 1695 (1984).
- [59] C. Ciraci, J. B. Pendry, and D. R. Smith, Hydrodynamic Model for Plasmonics: A Macroscopic Approach to a Microscopic Problem, *Chem. Phys. Chem.* **14**, 1109 (2013).
- [60] S. Raza, T. Christensen, M. Wubs, S. I. Bozhevolnyi, and N. A. Mortensen, Nonlocal response in thin-film waveguides: Loss versus nonlocality and breaking of complementarity, *Phys. Rev. B* **88**, 115401 (2013).
- [61] K. Busch, M. König, and J. Niegemann, Discontinuous Galerkin methods in nanophotonics, *Laser & Photonics Reviews* **5**, 773 (2011).
- [62] R. Esquivel and V. B. Svetovoy, Correction to the Casimir force due to the anomalous skin effect, *Phys. Rev. A* **69**, 062102 (2004).
- [63] D. Reiche, K. Busch, and F. Intravaia, Quantum Thermodynamics of Overdamped Modes in Local and Spatially Dispersive Materials, arXiv:1805.11353, online preprint (2018).
- [64] E. H. Hwang and S. Das Sarma, Linear-in- $T$  resistivity in dilute metals: A Fermi liquid perspective, *Phys. Rev. B* **99**, 085105 (2019).
- [65] V. B. Svetovoy and R. Esquivel, Nonlocal impedances and the Casimir entropy at low temperatures, *Phys. Rev. E* **72**, 036113 (2005).
- [66] V. B. Svetovoy, Application of the Lifshitz Theory to Poor Conductors, *Phys. Rev. Lett.* **101**, 163603 (2008).